# Absolute determination of local ground-state densities of atomic hydrogen in nonlocal-thermodynamic-equilibrium environments by two-photon polarization spectroscopy

R. Dux, K. Grützmacher, M. I. de la Rosa,* and B. Wende

*Physikalisch-Technische Bundesanstalt, Abbestrasse 2-12, D-10587 Berlin, Germany*

Two-photon polarization spectroscopy was applied in order to establish an absolute method for the determination of atomic ground-state densities in gases and plasmas. The method has high spatial and temporal resolution, can be used in a wide range of densities, and does not require any knowledge of the thermodynamic state of the system, because the measured two-photon absorption is strictly proportional to the atomic ground-state density. For atomic hydrogen, which is of basic physical importance as well as of great interest in technology and basic plasma research, the method has carefully been worked out. The measurement range is $N_H \geq 10^{19} \, \mathrm{m^{-3}}$ with an uncertainty of less than 10%. To achieve this accuracy, an arc plasma was shown to provide a standard of atomic hydrogen density with 5% uncertainty, and nonresonant two-photon absorption in xenon gas was established to serve as a transfer standard for easy application. In addition to the density measurements, the developed method allows for precise measurements of two-photon transition probabilities of other atomic species.

PACS number(s): 52.70.Kz, 06.20.Hq, 06.30.Dr

## I. INTRODUCTION

Complete understanding of the state of partially ionized plasmas has not yet been achieved, though this would allow for systematic optimization of technological processes utilizing plasmas or gases at high temperature. One of the reasons for this is the fact that reliable measurement methods for atomic number densities rarely exist though these have great influence on transport and rate coefficients of such plasmas. In particular, diagnostic tools are missing for quantitative density measurements of atoms in their ground state, which normally present the major part of the atomic density. Number densities of excited atoms can in principle be determined by emission spectroscopy, but the ground-state density can only be inferred from such measurements if the plasma is in local thermodynamic equilibrium (LTE), while plasmas of technological interest are usually far off LTE.

Various attempts were made to gain information about ground-state densities using laser spectroscopic techniques. For oxygen with its triplet structure of the ground state, ground-state atoms were detected by means of Raman spectroscopy [1] and coherent anti-Stokes Raman spectroscopy [2] spectroscopy. The signals were strongly superimposed by molecular resonances, however, which made reliable measurements nearly impossible. A more frequently used approach is optogalvanic

spectroscopy (resonantly enhanced multiphoton ionization) [3–5]: atoms are ionized by multiphoton absorption and the corresponding change of electrical conductivity is measured. However, the induced change of conductivity depends strongly on the plasma state and can hardly be analyzed quantitatively.

Laser-induced fluorescence was applied most often [6–16], especially in flames and microwave discharges. A suitable atomic level is populated by two-photon excitation, and the subsequent fluorescence radiation emitted during the decay on a one-photon transition is measured quantitatively. In environments with very low pressures ($p < 1 \, \mathrm{mbar}$), this is in principle a sensitive and quantitative method. With increasing pressure ($p > 10 \, \mathrm{mbar}$), the technique becomes subject to difficulties in deriving absolute atom number densities, because the fluorescence signal is quenched by various processes which can only be accounted for if the appropriate rate constants and the plasma state under investigation are well known. In atmospheric environments, these quenching processes become so dominant and complicated that quantitative measurements seem to be impossible. In general, the sensitivity of the method is decreasing with rising temperature and pressure because of the thermal background radiation from the plasma. In addition, radiative transport of the fluorescence light has to be considered at higher pressure.

To overcome the problems mentioned above, we applied an alternative method, which allows for a precise determination of atomic number densities by direct measurement of two-photon absorption. The method is well suited to be applied in a wide range of temperatures and pressures because the absorption integral is strictly proportional to the atomic number density and does not depend on the plasma parameters at all. The

---

*Permanent address: Universidad de Valladolid, Departamento de Física Aplicada III, Facultad de Ciencias, 47071 Valladolid, Spain.

high sensitivity required for the measurement of two-photon absorption is provided by the technique of two-photon polarization spectroscopy developed in our laboratory [17,18]. Because atomic hydrogen is of great importance for technological applications as well as for basic research in plasma physics, we worked out the method for the $1S \to 2S$ transition of atomic hydrogen.

## II. TWO-PHOTON POLARIZATION SPECTROSCOPY

The fundamental setup for measuring two-photon absorption by polarization spectroscopy is shown in Fig. 1. A circularly polarized pump beam of high irradiance is focused into the investigated plasma where it overlaps with a weak probe beam that is linearly polarized. The linear polarization of the probe beam can be thought of as a superposition of left and right circular polarization states. For an $S \to S$ transition only one of the two circular polarization components of the probe beam can excite a two-photon transition together with the pump beam, while the other circular component remains unchanged. For an arbitrary two-photon transition the two circular components will be absorbed differently. By this anisotropic absorption and the dispersion connected to it, the linear polarization of the probe beam is rotated and becomes slightly elliptic. These polarization changes can most sensitively be detected behind an analyzing polarizer set at a right angle with respect to the original polarization direction. For a probing signal beam with angular frequency $\omega_s$ and a pump beam with $\omega_p$ the first-order Doppler shift is reduced by a factor of $|\omega_s - \omega_p|/(\omega_s + \omega_p)$ if both beams are exactly counterpropagating. It should be mentioned that the spectroscopy method is quite similar to Raman-induced Kerr-effect spectroscopy [19].

The mathematical description of two-photon polarization spectroscopy is given in the Appendix. For an $S \to S$ transition the ratio of the signal beam irradiance behind the analyzing polarizer, $\delta E_s$, to the unperturbed irradiance before the interaction zone, $E_s$, is found to be

$$\frac{\delta E_s}{E_s} = \frac{1}{16}\left(\sigma_{S \to S}^{(2)} N \frac{\langle E_p l\rangle}{\hbar \omega_p}\right)^2 P(\Delta\omega) + R. \qquad (1)$$

Here, $N$ is the number density of the absorbing species (in units of $m^{-3}$), $\sigma^{(2)}$ is the frequency integrated two-photon absorption cross section (in units of $m^4$) and $\langle E_p l\rangle$ is a suitably defined mean value for the product of pump irradiance $E_p$ (in units of $W/m^2$) and the length $l$ of the overlap volume including the correlation function $g^{(2)}$ as well. $R$ denotes the residual transmission of the crossed polarizers, i.e., $\delta E_s/E_s$ as measured without pump beam. The line shape function $P(\Delta\omega)$ (in units of $s^2$) with $\Delta\omega = \omega_s - (\omega_0 - \omega_p)$ is the sum of the squares of the absorption and dispersion line shapes. Its explicit expression in terms of the two-photon absorption line profile is given in Eq. (A8) of the appendix. During the measurements on the hydrogen arc typical values for the quantities in Eq. (1) were $N = 7.5 \times 10^{22}\,m^{-3}$, $\langle E_p l\rangle = 5 \times 10^{12}\,W/m^2 \times 10^{-2}\,m$ and Lorentz line profiles with a full width $\Delta\nu = 100\,GHz$. With the hydrogen two-photon cross section $\sigma_{1S \to 2S}^{(2)} = 9 \times 10^{-43}\,m^4$ the signal in the line center results in a typical value of $\delta E_s/E_s = 10^{-5}$, being three orders of magnitude larger than the typical residual transmission $R = 10^{-8}$.

Equation (1) shows that the signal is proportional to the square of the atomic number density. The plasma conditions influence the signal only via the line shape function $P$, this can easily be accounted for by measuring the spectral line profile. In the center of a symmetric line, the dispersion part of the signal vanishes and the signal is proportional to the square of the two-photon absorption line profile.

If Eq. (1) were directly to be used for the determination of absolute number densities, the value of $\langle E_p l\rangle$ and the atomic cross section $\sigma^{(2)}$ had to be known. Even if $\sigma^{(2)}$ is available, $\langle E_p l\rangle$ still depends on a number of parameters: the pulse energy of the pump beam, the temporal pulse shapes, the irradiance distributions of both laser beams in the focus, and the spatial and temporal overlap of the focused beams, which can hardly be measured. Therefore, direct use of Eq. (1) is not reasonable.

However, if $\langle E_p l\rangle$ can be kept constant with sufficient long term stability, a precise determination of the atomic number density $N$ can be performed by a relative measurement with respect to a standard of number density for the atomic species concerned. Provided that such a standard (subscript st) is available, Eq. (1) with $\langle E_p l\rangle = $ const yields

$$\frac{N}{N_{st}} = \left[\frac{(\delta E_s/E_s) - R}{(\delta E_s/E_s)_{st} - R}\frac{P_{st}(\Delta\omega)}{P(\Delta\omega)}\right]^{\frac{1}{2}} \qquad (2)$$

for the density ratio. This ratio is independent of $\sigma^{(2)}$ and of all laser beam parameters that determine the overlap, including the two-photon correlation. Therefore, the aim of this work was to establish a standard of atomic hydrogen densities and to demonstrate the precision that can be reached by this measurement technique.
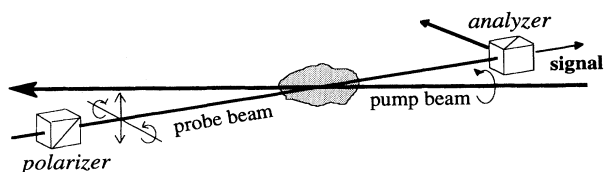


FIG. 1. The principal setup of two-photon polarization spectroscopy. The probe beam's linear polarization is turned and becomes slightly elliptic due to anisotropic absorption and dispersion when exciting a two-photon transition together with the circularly polarized pump beam. The polarization changes are detected behind an analyzer set at right angle with respect to the polarizer.

## III. EXPERIMENTAL SETUP

Our experimental setup is shown in Fig. 2. The pump beam is generated by a KrF*-excimer laser with oscillator amplifier design (Lambda Physik, EMG150EST),
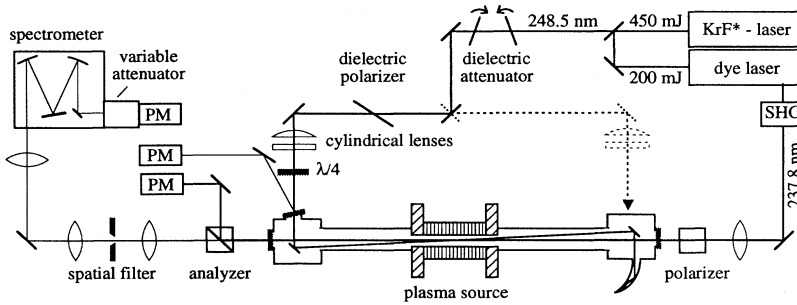
FIG. 2. The scheme of the experimental setup shows in detail the arrangement of all optical components for preparing and handling of the counterpropagating pump and probe beam. The dashed line indicates the modification for colinear beams.

which can produce pulse energies of 450 mJ in 20 ns at a wavelength of $\lambda = 248.5$ nm with spectral resolution $\Delta\nu = 5.5$ GHz [full width at half maximum (FWHM)]. A part of this beam is used to pump a dye laser (Lambda Physik, FL2003E), which is equipped with an intracavity étalon and a frequency doubling unit using $\beta$-barium borate. The probe beam from this laser is tuned around $\lambda = 237.8$ nm for the excitation of the $1S \rightarrow 2S$ transition of hydrogen and around $\lambda = 250.8$ nm for the xenon transition $5p^6\,{}^1S_0 \rightarrow 5p^5\,6p\,[1/2]_0$ with spectral resolution $\Delta\nu = 1.1$ GHz (FWHM). With this laser combination a high detection sensitivity can be achieved because of the high pulse energy of the pump laser providing an irradiance up to $2$ GW/cm$^2$ in the focus of a 1 m lens. On the other hand, the small frequency difference of the two lasers results in a residual Doppler width that is only 2.3% of its original value when exciting hydrogen by counterpropagating beams. For simplicity we refer to this as "Doppler-free" excitation throughout the text.

The pump beam, whose energy can be attenuated by a pair of angle-dependent partial reflectors, is sent through a circular polarizer consisting of a dielectric linear polarizer and a zero-order $\lambda/4$ plate. The circular polarization state of the pump beam was measured to contain less than 1% of the wrong (opposite) circular polarization which is sufficient for this type of measurements as discussed in the appendix [see the paragraph following Eq. (A7)]. The pump beam is focused by two cylindrical lenses, thus compensating for the astigmatism of the excimer laser beam. For the measurements reported here the focus overlap had typical dimensions of $l = 10$ mm and $\emptyset = 150\,\mu$m. For better shot to shot reproducibility the pump beam focus is set to be 1.5 times larger than the focus of the probe beam. The pump beam direction can be chosen colinear or counterpropagating to the probe beam, allowing for the measurement of Doppler-broadened or Doppler-reduced line shapes.

Behind the focusing lens (1 m) the probe beam passes through the linear polarizer, the input and the output windows of the plasma chamber, and the polarization analyzer. The signal is detected by a photomultiplier behind a spatial and spectral filter. Polarizer and analyzer are air spaced Glan polarizers (Bernhard Halle Nachfl.), and the perfect crossing angle between them can be controlled within an uncertainty of 1 $\mu$rad. For the total setup, a residual probe beam transmission down to $2 \times 10^{-9}$ was achieved. Even at this low signal level, stray light from the strong pump beam was still negligi-

ble with respect to the signal. In order to achieve such a small residual transmission it is essential that the pump and the probe beam pass through different windows (see Fig. 2) and that the polarizers and the windows closing the plasma chamber are free of mechanical stress. Special care was taken to avoid inhomogeneous illumination of the windows by plasma radiation. When running the experiment for about 5 h, the residual transmission increased to about $2 \times 10^{-8}$ due to irreversible radiation damage of the windows. Under the realistic assumption that signals can still be detected that are 10% of the residual transmission level, probe beam absorptions down to $5 \times 10^{-5}$ could be measured.

Adaptation of the signal level to the dynamic range of the pulse electronics was performed by attenuating the light with different combinations of stray plates and pinholes imaging the laser profile on the photocathode of the photomultiplier. The attenuation unit was equipped with 90° turning magnets, and allowed one to change the attenuation factor within one scan by five orders of magnitude in seven steps. Two other photomultipliers supplied reference signals for the pulse energies of pump and probe beam. With the setup described, measurements were performed on xenon in a simple gas cell and on a hydrogen plasma generated in a wall-stabilized, steady-state arc discharge.

## IV. PRIMARY INVESTIGATIONS

As a first step to check the experimental setup, we investigated the dependence of the polarization signal on the atomic number density $N$ and the pump irradiance $E_p$. For this purpose, we made use of the well known two-photon transition $5p^6\,{}^1S_0 \rightarrow 5p^5\,6p\,[1/2]_0$ of xenon [22,23]. Since this transition starts from the ground state, the number density of absorbing atoms is simply given by the pressure of the rare gas at room temperature.

Figure 3 shows spectra recorded at various xenon gas pressures from 10 to 500 mbar, while keeping the pump irradiance and overlap geometry constant. A setup with counterpropagating beams was used, and each spectrum shown is the mean of signals measured with left and right circularly polarized pump beam. Minor influences on the signal caused by residual anisotropy of the window material cancel out this way [see Eq. (A7) and the related paragraph]. The signal heights vary by four orders of magnitude, and the linewidth increases with
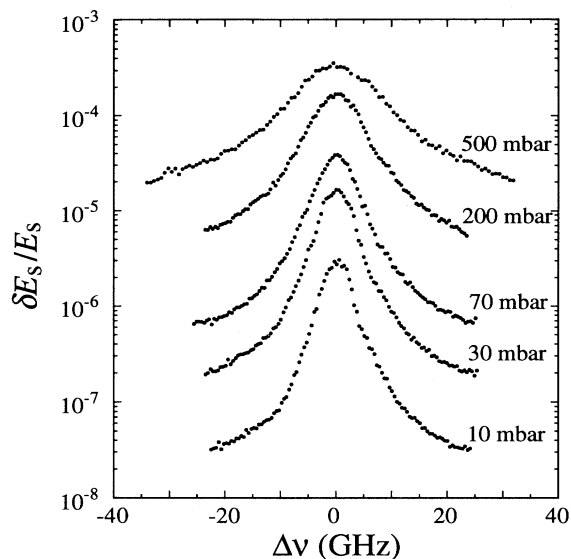
FIG. 3. Set of Doppler-free two-photon polarization spectra of the xenon transition $5p^6\,{}^1S_0 \to 5p^5\,6p\,[1/2]_0$ for different gas pressures. Pump irradiance and overlap geometry were kept constant in order to obtain the variation of number density from the absolute signal heights. Pressure broadening increases the linewidth of the resonance as the pressure is increased.
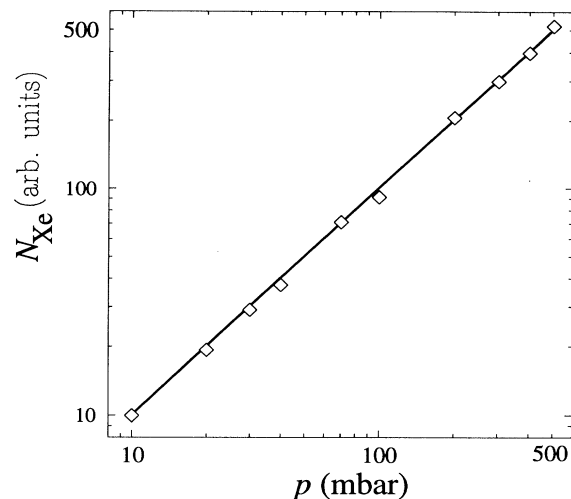
FIG. 4. Experimentally derived relative number densities of xenon atoms as a function of gas pressure. The xenon number densities were evaluated from the spectra of Fig. 3. The straight-line fit gives the expected proportionality $N \propto p$.

pressure. Pressure broadening of this xenon transition has been investigated experimentally [22,24] as well as theoretically [25,26] and has been shown to cause an asymmetric Lorentz profile as given in Eq. (A11), plus an additional redshift of the line center. The redshift $\Delta\nu/p = -8$ GHz/bar is suppressed in Fig. 3. At 10 mbar the linewidth is dominated by the lasers and the profile can be described by a transformed Gaussian profile, Eq. (A9), with FWHM of 5.6 GHz. For the higher pressures a transformed Voigt profile according to Eq. (A9) with fixed Gauss width was used to fit the data points. The pressure broadening was evaluated to produce a FWHM of 19 GHz/bar in good agreement with the result of Raymond et al. [22] who give 18.5 GHz/bar. Isotope shifts of about 300 MHz remain unresolved [24].

Line shape factors were evaluated from the fit parameters of the transformed Voigt profiles. As discussed in the Appendix, polarization spectroscopy hides the asymmetry of the underlying absorption profile. In order to account for the hidden asymmetry, two-beam two-photon absorption spectroscopy was carried out at higher pressures. For this purpose, we used an unfocused pump beam with cross section of about 4 mm × 4 mm overlapping for about half a meter with an unfocused probe beam (2 mm in diameter). Polarizer and analyzer for the probe beam were set parallel, and the pump beam was kept linearly polarized. We observed only minor asymmetries in the pressure range of 500 mbar. The asymmetry factor $\kappa$ is of the order of 10% at 500 mbar, and the corresponding correction [see discussion of Eq. (A11)] is negligible. Thus, relative number densities $N$ could be

derived from the signal heights and the line shape parameters. They are plotted versus gas pressure on a double logarithmic scale in Fig. 4. The solid line is the result of a least square fit with trial function $N \propto p^\alpha$. The exponent $\alpha$ was found to be $1.000 \pm 0.002$. This demonstrates that the experimental setup does in fact produce signals proportional to $N^2$ according to Eq. (1).

We also tested the dependence of two-photon absorption on the pump beam irradiance $E_p$. Here, the proportionality was proved within $\pm 2\%$ up to the highest achievable irradiances of 2 GW/cm$^2$.

As these experiments show, Eq. (1) gives the correct theoretical description of two-photon spectroscopy under the conditions of our experiment, so that the setup is well suited for relative density determinations, i.e., the overlap parameter $\langle E_p l \rangle$ can be kept constant with sufficient long term stability (typically 10 h). Absolute measurements of xenon number densities according to Eq. (2) can thus be easily performed using a simple gas cell as number density standard.

## V. A HYDROGEN ARC AS A NUMBER DENSITY STANDARD OF ATOMIC HYDROGEN

The basic idea to establish the number density standard is to generate a hydrogen plasma which consists mainly of atomic hydrogen ($N_H \gg N_{H_2}, N_e$) and thus is a nearly ideal atomic gas. Then, the atomic density can be determined by measurements of pressure and gas temperature. The gas temperature can be deduced from Doppler-free and Doppler-broadened two-photon spectra if the Doppler width is large enough compared to the Stark width. This sets another upper limit on the electron density of the plasma. A rough estimate of plasma composition in thermodynamic equilibrium, which uses

the law of mass action and the Saha equation to determine the degrees of dissociation and ionization, indicates that an atomic hydrogen plasma with sufficiently small electron density may be found at low plasma pressures not exceeding 100 mbar and temperatures above about 5000 K.

We chose a commonly used, wall-stabilized cascaded arc [27] operated with pure hydrogen at a pressure of 100 mbar to generate such a plasma. The dimensions of the arc chamber were 100 mm in length and 8 mm in diameter which is sufficiently large with respect to the spatial resolution provided by the laser spectroscopic setup. The current varied from 18 to 63 A, the typical voltage drop in the column was 5 kV/m, and the maximum dc power fed into the plasma chamber was about 40 kW. This wall stabilized arc is a very reliable plasma source. Setting the pressure, the gas flow and the current to predefined values, the voltage drop in the arc column is reproduced within 0.5%, even if the arc chamber is disassembled and put together again several times in between. The arc provides excellent long term stability and reproducibility (main requirements for a standard) and allows for large variation of the plasma parameters.

It is well known, however, that a hydrogen plasma with $p = 100$ mbar and $T < 10\,000$ K obeys partial LTE only, i.e., the heavy particles (molecules, atoms and ions) have the same kinetic temperature $T_g$, but the electrons have a slightly higher temperature $T_e$, because they are ohmically heated and need many collisions to transfer their energy to the heavy particles. Considering singly ionized species only and using $N_i = N_e$, Dalton's law is

$$\frac{p}{k_B T_g} = N_H + N_{H_2} + N_e \left(1 + \frac{T_e}{T_g}\right). \qquad (3)$$

In general, knowledge of $T_g$, $N_{H_2}$, $N_e$, and $T_e$ is required, in addition to $p$, to obtain $N_H$ from this equation, unless $N_{H_2}$ and/or $N_e$ can be shown to be negligible in comparison with $N_H$ for particular plasma parameters. For the corresponding measurements that are described in the following, the pressure was held at 100 mbar with 1% uncertainty.

The temperature $T_g$ of heavy particles was evaluated by deconvolution of Doppler-free from Doppler-broadened $1S \to 2S$ spectra measured with counter-propagating and colinear two-photon polarization spectroscopy, respectively. Two typical pairs of line shapes normalized to the same maximum signal are shown in Fig. 5, one pair of scans measured on the plasma axis, and the other one at 2 mm off axis. The solid lines represent least square fits to the data with a polarization line shape $P$ which corresponds, via Eq. (A9), to a Voigt absorption profile. From the increase of the width of the Gauss contribution we could evaluate the kinetic temperature of atomic hydrogen using its well known square root dependence on temperature. The precision of this temperature determination is high for large changes of the linewidth when switching from the Doppler-free to the Doppler-broadened scan, i.e., for narrow Doppler-free spectra. The uncertainty increased with temperature from 3.1 to 3.9%. For the estimation of the final

uncertainty, it was taken to be 4% throughout.

The contribution of charged particles in Eq. (3) is given by the last term. For a weakly ionized plasma, this contribution is small. It was determined by measurements of $N_e$ and $T_e$. $N_e$ was obtained from the Stark broadening of the $2S$ level given by the Doppler-free width of the $1S \to 2S$ spectra. $T_e$ and another value of $N_e$ were determined by quantitative emission spectroscopy of the Balmer lines. A 1 m double monochromator was used to compare the spectral radiance of the plasma and a calibrated tungsten strip lamp. The plasma was observed end on with relative aperture 1:100. Absorption measurements showed that the spectral lines $H_\beta$, $H_\gamma$, and $H_\delta$ were optically thin. The values of electron density obtained from the Stark broadening of the $2S$ level [28] and of $H_\gamma$ [29] agree within less than 10%, and the electron density was found to contribute at most only 3% of the total particle density. $T_e$ was deduced as the Boltzmann temperature for the atomic levels $n=4$–6 and was found to be about 15% higher than $T_g$. This is in good agreement with an estimate of the energy gained by an
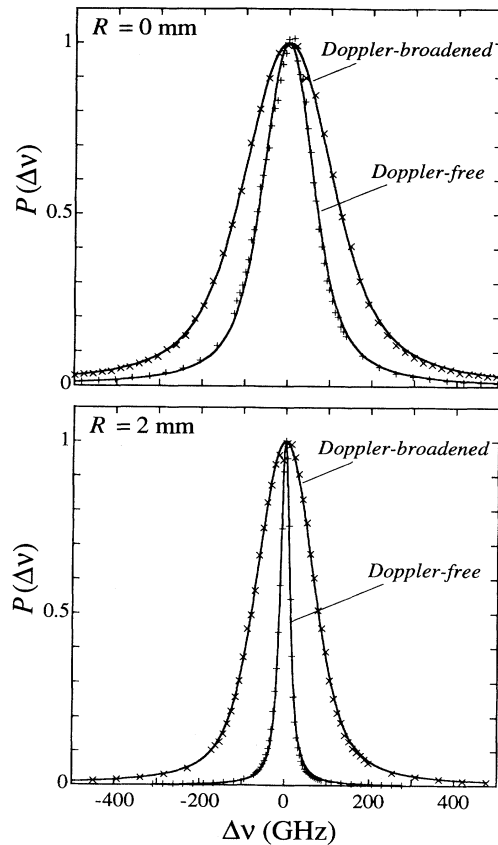


FIG. 5. Doppler-broadened ($\times$) and Doppler-free ($+$) polarization line shapes of the hydrogen $1S \to 2S$ transition. The line shapes were measured with copropagating and counterpropagating two-photon polarization spectroscopy, respectively, on the axis and 2 mm off axis of the plasma column at a discharge current of 45 A. The solid lines are least square fits to the data with transformed Voigt absorption profiles.
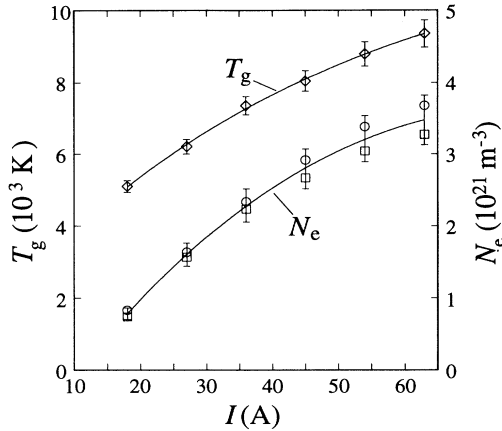
FIG. 6. Temperatures from the Doppler broadening of the $1S \rightarrow 2S$ transition ($\diamond$) and electron densities from the Stark broadening of the $1S \rightarrow 2S$ transition ($\square$) and of the $H_\gamma$ line ($\circ$) on the axis of the plasma column at a pressure of $p = 100$ mbar for different plasma currents.

electron along a mean free pass in the external electric field driving the plasma current. For the further evaluation, we set $T_e = T_g$, since even a 50% deviation of $T_e$ from $T_g$ is irrelevant because of the small contribution of the electron density to Eq. (3). In Fig. 6, the kinetic temperature of atomic hydrogen and the electron density on the plasma axis are shown as functions of the plasma current.

To obtain the density $N_H$ of atomic hydrogen from Eq. (3), it remains to determine the density $N_{H_2}$ of molecular hydrogen or to show that it is completely negligible at sufficiently high temperatures. In the later case, Eq. (3) becomes

$$\frac{p}{k_B T_g} = N_H + 2N_e. \qquad (4)$$

To investigate whether complete molecular dissociation was attained in our plasma, we used the measured integrals of the two-photon absorption line shapes to determine the relative variation of atomic number density over the whole temperature range $T_g = 5200$ K–9400 K. Assuming zero molecular density at the highest temperature, the relative values can be converted to absolute atomic number densities via Eq. (4). Comparison of $N_H + 2N_e$ with $p/k_B T_g$ clearly proves that Eq. (4) does in fact hold down to a temperature of about 8000 K (see Fig. 7), and allows for a determination of $N_H$ by measurements of $p$, $T_g$, and $N_e$. Below this temperature, hydrogen is no longer purely atomic, and the difference between the upper and lower curve in Fig. 7 is the density of molecules in the plasma. Thus, for temperatures $T_g = 8000$ K–9400 K, Eq. (4) is valid to determine absolute atomic number densities of the hydrogen standard.

As a conclusion, these measurements establish that the plasma on the axis of the wall-stabilized arc at a pressure of 100 mbar is a standard of atomic hydrogen densities for temperatures of 8000 K–9400 K with corresponding number densities of $8.4 \times 10^{22}$ m$^{-3}$ to $7.0 \times 10^{22}$ m$^{-3}$ according
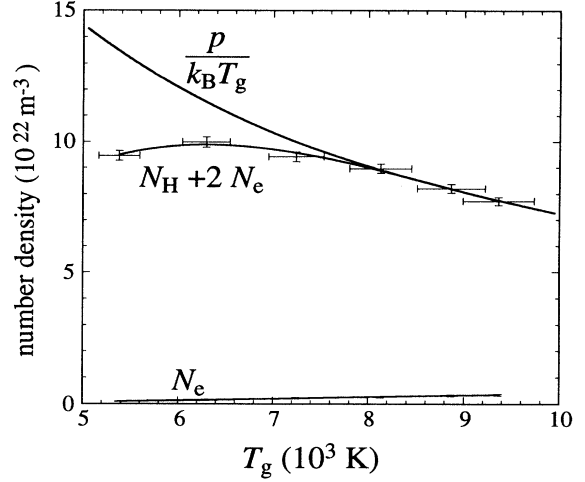


FIG. 7. Comparison of number densities versus kinetic gas temperature $T_g$ for $p = 100$ mbar on the axis of the plasma column. The upper line represents the ideal gas isobar, giving the total number density of all particles at a given temperature. For $T_g > 8000$ K it shows the same behavior as the $(N_H + 2N_e)$ line, indicating that the molecular hydrogen is completely dissociated. At lower temperatures the number density of molecules is given by the difference of the two curves. Additionally the small contribution of $N_e$ is shown at the bottom.

to Eq. (4), with a total uncertainty of 5% as calculated from the partial uncertainties discussed above: the measurement of $T_g$ contributes 4% as the main part, while the measurements of $p$, $N_e$, and $T_e$ lead only to a 1% increase of the total uncertainty.

## VI. MEASUREMENT OF RADIAL DISTRIBUTIONS IN THE PLASMA COLUMN

The arc measurements were not only carried out on the axis of the plasma column. Temperatures, electron densities, and atomic densities were also determined in a radial range of $\pm 2$ mm out of the axis. For two different plasma currents, radial profiles for the number densities of the different species are shown in Fig. 8(a) and the corresponding temperature distributions in Fig. 8(b). These distributions illustrate that complete dissociation on the axis is only achieved at nearly twice the temperature of 4500 K which would be required in LTE, and that a purely atomic hydrogen gas is found only in a small region around the axis. The radial temperature and concentration gradients in the arc drive diffusion currents that increase the molecular concentration on the axis compared with the equilibrium value. On the other hand, as soon as the molecular concentration goes down, there is a steep rise in the temperature distribution because the heat conductivity decreases drastically if the energy input is no longer consumed by the dissociation of molecules. These features are well known from previous investigations of hydrogen arcs [30,31].
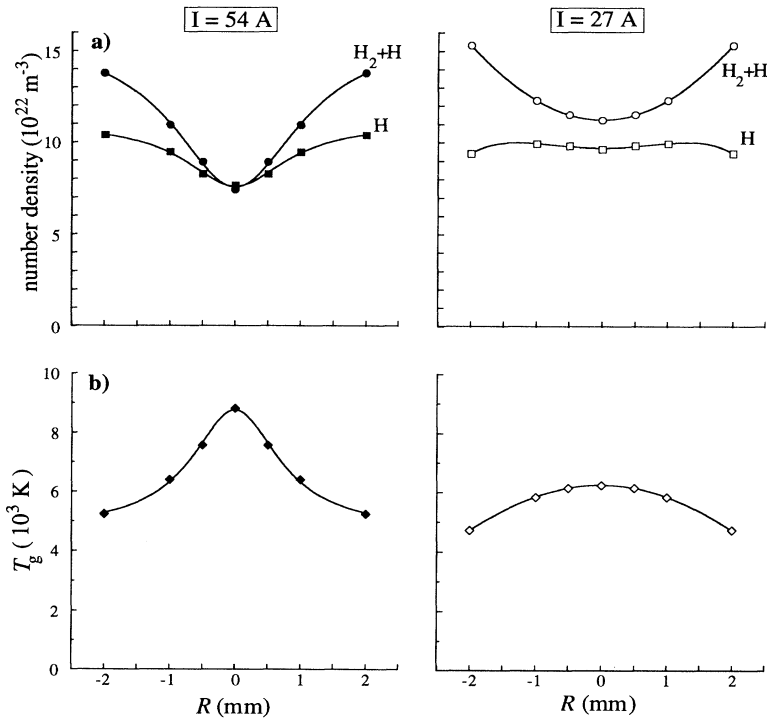
FIG. 8. Radial distributions of (a) neutrals and atoms, and (b) the corresponding temperatures for plasma currents of $I = 27$ A (right) and $I = 54$ A (left).

When measuring the atomic density in plasma regions with high molecular concentration, high irradiances of the pump beam may possibly cause an extra atomic density by photodissociation of molecules and thus lead to two-photon absorption growing stronger than linear with pump irradiance. To investigate this question we measured the polarization signals for different pump irradiances in a region with 50% molecular concentration. Figure 9 shows two-photon absorption versus pump irradiance. No deviation from the linear behavior is found up to the highest pump irradiances of nearly $2\,\mathrm{GW/cm^2}$. In another experiment with purely molecular hydrogen gas under atmospheric pressure at room temperature, no polarization signal could be detected at the $1S \rightarrow 2S$ resonance of atomic hydrogen. Therefore, up to an irradiance of $2\,\mathrm{GW/cm^2}$, laser induced photodissociation is not a source of error for the density determination.

## VII. XENON AS A TRANSFER STANDARD OF ATOMIC HYDROGEN DENSITIES

For application of the measurement technique in other laboratories, the hydrogen density standard is too complicated, because it needs a lot of experimental equipment. It should therefore be substituted by a transfer standard that is more easily manageable but still precise. Such a transfer standard can be based on nonresonant two-photon absorption in xenon at the wavelength of the hydrogen $1S \rightarrow 2S$ transition (partially caused by the far wing of the transition $5p^6\,^1S_0 \rightarrow 5p^5\,6p\,[1/2]_0$). For a xenon pressure of 500 mbar at room temperature, polar-

ization spectroscopy yields sufficiently high signals at the same excitation conditions as used for plasma diagnostic. As its main advantage, the xenon reference requires no change of the frequency of the tunable probe laser so that the focus overlap of the two beams represented by $\langle E_p l \rangle$ remains unchanged during a comparison.

The nonresonant polarization signal obtained from xenon at the wavelength of the hydrogen $1S \rightarrow 2S$ tran-
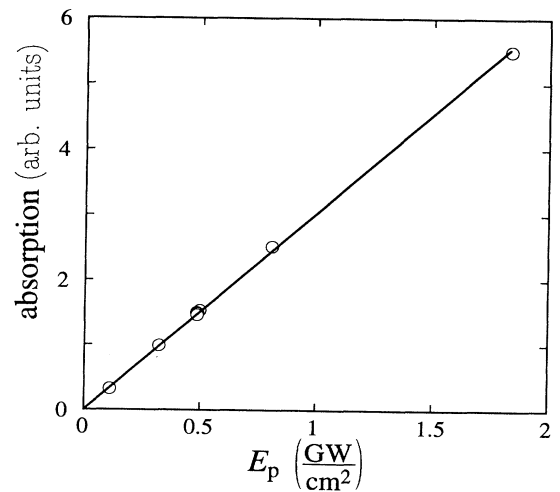


FIG. 9. Absorption on the $1S \rightarrow 2S$ transition is found to be proportional to the pump irradiance $E_p$. No extra contribution to the signal by photodissociation of hydrogen molecules could be observed.

sition shows the same dependence on particle density and pump irradiance as a resonant one. To account for a non-resonant polarization signal, the two-photon cross section and the line shape function $\sigma^{(2)}\sqrt{P(\Delta\omega)}$ can be substituted by a constant factor $c_{Xe}$ with SI unit m$^4$ s:

$$\frac{\delta E_s}{E_s} = \frac{1}{16}\left(c_{Xe}N_{Xe}\frac{\langle E_p l\rangle}{\hbar\omega_p}\right)^2 + R. \tag{5}$$

This equation was experimentally proved for a wide range of xenon pressures up to 500 mbar at room temperature and pump irradiances up to 2 GW/cm$^2$. No spectral dependence could be detected in a frequency range of $\delta\nu = \pm 100$ GHz making $c_{Xe}$ independent of laser bandwidth. The closest two-photon resonance of xenon is 65 THz away from this frequency range and has a linewidth around 10 GHz in this pressure range. It cannot cause changes of $c_{Xe}$, because for polarization spectroscopy the far wing of the line shape does not depend on the line width and decreases as $1/(\pi\Delta\omega)^2$ [see Eq. (A11)]. At xenon pressures above 500 mbar weak deviations of Eq. (5) might be expected due to the increasing asymmetry factor $\kappa$ in Eq. (A11). A comparison of the signals obtained from xenon and hydrogen yields an equation similar to Eq. (2):

$$\frac{c_{Xe}}{\sigma^{(2)}} = \frac{N_H}{N_{Xe}}\left[\frac{(\delta E_s/E_s)_{Xe} - R}{(\delta E_s/E_s)_H - R}P_H(\Delta\omega)\right]^{\frac{1}{2}}. \tag{6}$$

The calibration constant $K_{Xe-H} = c_{Xe}/\sigma^{(2)}$ can be determined by comparison of xenon and the hydrogen standard. On the other hand, knowledge of this calibration constant allows to determine hydrogen densities with respect to xenon densities.

For the determination of $K_{Xe-H}$, six sets of measurements were performed. We always started by filling xenon into the plasma chamber and measured the nonresonant signal at a number of different pump irradiances. Then we switched on the plasma, measured the resonant hydrogen signal with the standard, switched off the plasma and again filled xenon gas into the plasma chamber for a second comparison. From these measurements the calibration constant was determined with 6% uncertainty to be $K_{Xe-H} = (1.168 \pm 0.066) \times 10^{-15}$ s. The uncertainty is dominated by the uncertainty of the standard density and only weakly by the statistical error of the comparison itself (2.5%).

As already mentioned above, the value of the calibration constant does not depend on laser bandwidths since it has no spectral dependence. However, the precise determination of hydrogen densities depends on the line shape function of the hydrogen resonance $P_H(\Delta\omega)$, which has to be measured carefully. If the hydrogen resonance is very narrow this must include a measurement of laser widths. The evaluation procedure for $N_H$ may be checked by two independent sets of measurements. A measurement with counterpropagating laser beams ("Doppler-free" line shape) and a measurement with colinear beams (Doppler-broadened line shape) have to result in the same hydrogen number density.

## VIII. FIELDS OF APPLICATION

With respect to the measurement of atomic densities, we first focus on hydrogen. Using xenon as transfer standard it is now possible to perform determinations with an uncertainty well below 10%. The accessible range of number densities depends on the pump irradiance $E_p$, the absorption length $l$ and the residual transmission $R$. For a Lorentzian line shape with full width $\Gamma$ around $\omega_0$ and assuming a detection limit of $R/10$, we find as a lower limit for $N_H$:

$$N_H \geq 2.8 \times 10^{19}\,\text{m}^{-3}$$
$$\times\left(\frac{E_p}{\text{GW/cm}^2}\frac{l}{\text{cm}}\right)^{-1}\left(\frac{10^6\Gamma}{\omega_0}\right)\left(\frac{R}{10^{-8}}\right)^{1/2}. \tag{7}$$

This follows directly from Eq. (1), using the two-photon cross section $\sigma^{(2)} = 8.975 \times 10^{-43}$ m$^4$ [32]. It also holds for other laser combinations, e.g., the fourth harmonic of a Nd:Yag laser at 266 nm together with a frequency doubled dye laser at 220 nm, because the two-photon cross section for the $1S \rightarrow 2S$ transition (without intermediate level) depends only very weakly on the frequency combination if $\omega_1 \approx \omega_2$ [32]. For a hydrogen flame at atmospheric pressure and a typical temperature of about 2000 K, a minimum detection limit of $N_H = 10^{19}$ m$^{-3}$ represents a fraction of 3 ppm. For the detection limit with high pump irradiance, one has to take into account that the linewidth is increased by photoionization of the $2S$ level and the ac-Stark effect. According to Ditchburn [33], photoionization causes an extra Lorentzian width of $\Gamma_{ion} = 4 \times 10^{-7}\omega_0 E_p/(\text{GW/cm}^2)$.

Single shot measurements in nonstationary plasmas require lasers with high shot-to-shot stability. In our experiment, with the signal electronics integrating over one laser shot, we could already achieve a 12% standard deviation for the single shot measurement indicating that the shot to shot variation of the probe volume (given by the focal overlap of pump and probe beam) and the spectral and temporal quality can be kept fairly constant. Better results may be achieved with single longitudinal mode lasers.

In this work, we always measured the whole line profile to obtain information about atomic and electron density and temperature. If signal levels are large enough, density ratios can more simply be determined by measuring at a fixed frequency in the wing of the polarization line shape, which is always given by $1/(\pi\Delta\omega)^2$, independent of the central line shape of the resonance, i.e., independent of plasma parameters.

In general, the excitation should preferably be performed by a high-energy fixed-frequency pump laser combined with a tunable laser for the signal beam. Sufficient pump irradiances $E_p$ can thus be produced to reach high sensitivity. Depopulation of the ground state cannot be caused by the off-resonant pump beam itself. Spectral filtering of the signal beam helps to suppress straylight from the strong pump beam, and photon correlation effects cancel when using two independent light sources.

The method may also be applied to the measurement of other important species like O(112.9 nm), N(105.5 nm),

and C(140.2 nm). For absolute measurements, density standards for these species are required. Gas titration methods [34] might be considered, but do not seem to provide appropriate particle densities. However, arc plasmas similar to the one we applied for H should also be feasible at least in the cases of C and N.

Another important application of the method is the measurement of atomic two-photon cross sections, many of which are still unknown, by reference to the exact value of the hydrogen cross section. Measurements of two-photon cross sections for a set of xenon transitions have been performed and will be published elsewhere.

## IX. SUMMARY

We presented a method for the determination of atomic number densities by the measurement of two-photon absorption. The high sensitivity required for the measurement of two-photon absorption is accomplished by a spectroscopic method based on the polarization change of a linearly polarized analyzing beam which is caused by the excitation of a two-photon transition in the overlap volume with a circularly polarized pump beam.

The main features of the method are

measurement range: $N \geq 10^{19}\,\mathrm{m}^{-3}$ (for hydrogen);
uncertainty:      $< 10\%$;
temporal resolution: typical 5 ns;
spatial resolution:    typical probe volume:
          $\emptyset = 150\,\mu\mathrm{m}$, $l = 10\,\mathrm{mm}$.

For the determination of atomic densities in plasmas and gases at high temperature, the technique has a number of advantages compared to former methods.

No additional information is needed about the state of the plasma (pressure, temperature, or chemical composition).

The method does not rely on the assumption of local-thermodynamic equilibrium.

The method is applicable in high temperature environments with unchanged sensitivity, by operating in a Doppler-free configuration.

The sensitivity is not restricted by the thermal radiation of the plasma.

The signal carried by the probe beam can be detected at great distances from the point of measurement.

Thus, the method allows for precise measurements of the atomic densities in a formerly inaccessible range of plasma parameters. For those parameters that are within

the reach of laser induced fluorescence as well, the uncertainty is decreased by an order of magnitude for atomic hydrogen [11]. This small uncertainty can be achieved for all atomic species for which a density standard of corresponding precision can be developed.

## ACKNOWLEDGMENTS

## APPENDIX: MATHEMATICAL DESCRIPTION

The mathematical description of two-photon absorption and polarization spectroscopy given here is directly based on the atomic two-photon transition rate as calculated by second-order perturbation theory. Alternatively, the description could be given in terms of the third-order nonlinear susceptibility. The connection of these approaches can be found in Refs. [20] and [35]. An introduction to polarization spectroscopy is given in Ref. [36].

The excitation rate per atom for a transition $i \to f$ induced by two copropagating or counterpropagating beams with irradiances $E_{1,2}$ (SI unit W/m$^2$) and polarizations $\vec{e}_{1,2}$ can be expressed as

$$W_{if}^{(2)} = \sigma_{if}^{(2)}(\vec{e}_1, \vec{e}_2)\frac{E_1}{\hbar\omega_1}\frac{E_2}{\hbar\omega_2}L(\omega_1 + \omega_2 - \omega_0)g^{(2)}, \quad \text{(A1)}$$

where $\sigma_{if}^{(2)}(\vec{e}_1, \vec{e}_2)$ is the frequency-integrated two-photon absorption cross section (SI-unit m$^4$). $L(\omega_1+\omega_2-\omega_0)$ (SI unit s) is the line shape function of the atomic transition (normalized to unit area) with resonance frequency $\omega_0$. The dimensionless factor $g^{(2)}$ describes the second-order correlation function for the two beams. For weak absorption, $g^{(2)}$ is constant during the whole interaction time and equals 1 for statistically independent beams [20,21].

The two-photon cross section depends on the polarizations of the exciting laser beams since it is (in electric dipole approximation)

$$\sigma_{if}^{(2)}(\vec{e}_1, \vec{e}_2) = \frac{\pi e^4}{2\epsilon_0^2 c^2}\omega_1\omega_2 \left| \sum_n \frac{\left(\vec{R}_{fn}\cdot\vec{e}_2\right)\left(\vec{R}_{ni}\cdot\vec{e}_1\right)}{E_n - \hbar\omega_1} + \frac{\left(\vec{R}_{fn}\cdot\vec{e}_1\right)\left(\vec{R}_{ni}\cdot\vec{e}_2\right)}{E_n - \hbar\omega_2} \right|^2. \quad \text{(A2)}$$

For transitions starting from a state with $J_i = 0$ or, in the case of $LS$ coupling, with $L_i = 0$, the polarization dependence of the cross section can explicitly be calculated. With the direction of the laser beams taken as the $z$ axis (quantization axis), the polarizations are linear combinations $\vec{e} = \epsilon^+\vec{e}_+ + \epsilon^-\vec{e}_-$ of the spherical unit vectors $\vec{e}_\pm$. Spherical decomposition of the matrix elements in Eq. (A2) according to the Wigner-Eckart theorem leads to

$$\sigma_{if}^{(2)}(\vec{e}_1, \vec{e}_2) = \sigma_{if}^{(2)} \left| \epsilon_1^+ \epsilon_2^- + \epsilon_1^- \epsilon_2^+ \right|^2, \quad J = 0 \rightarrow 0$$

$$\sigma_{if}^{(2)}(\vec{e}_1, \vec{e}_2) = \sigma_{if}^{(2)} \left[ \frac{1}{4} \left| \epsilon_1^+ \epsilon_2^- + \epsilon_1^- \epsilon_2^+ \right|^2 + \frac{3}{2} \left( \left| \epsilon_1^+ \epsilon_2^+ \right|^2 + \left| \epsilon_1^- \epsilon_2^- \right|^2 \right) \right], \quad J = 0 \rightarrow 2 \qquad \text{(A3)}$$

where $\sigma_{if}^{(2)}$ denotes the cross section for two laser beams with identical linear polarizations, e.g., $\epsilon^+ = \epsilon^- = 1/\sqrt{2}$. In two-photon polarization spectroscopy, beam 1 is an intense pump beam (index $p$) with circular polarization, say $\vec{e}_+$, and beam 2 is the weak probing signal beam (index $s$) with polarization $\vec{e}_x$. For an $S \rightarrow S$ transition, only the $\vec{e}_-$ component of the probe beam can induce a two-photon excitation. For an $S \rightarrow D$ transition, on the other hand, it is predominantly the $\vec{e}_+$ component. The absorption of the probe beam in a thin layer with number density $N_i$ of the initial state and negligible population of the final state, which is irradiated by the pump beam, is given by $W_{if}^{(2)} \hbar \omega_s N_i = dE_s/dz = -\alpha_s(\omega_s) E_s$. From this the spectral absorption coefficient $\alpha_s(\omega_s)$ for the probe beam is found to be

$$\alpha_s(\omega_s) = \sigma_{if}^{(2)}(\vec{e}_+, \vec{e}_x) N_i \frac{E_p}{\hbar \omega_p} L(\Delta\omega) g^{(2)}, \qquad \text{(A4)}$$

where $\Delta\omega$ is an abbreviation for $(\omega_s + \omega_p - \omega_0)$. From Eq. (A4) the complex index of refraction due to two-photon excitation, $\Delta\eta_s = \Delta n_s + i\Delta\kappa_s$, can be calculated for the probe beam. Its imaginary part is $\alpha_s c_0/2\omega_s$ and the real part results from the Kramers-Kronig relation. For the case of the hydrogen $1S \rightarrow 2S$ transition, $\Delta\eta_s$ applies to the $\vec{e}_-$ component only, and is constant throughout the interaction zone, because the pump irradiance $E_p$ is not noticeably attenuated. In the weak absorption approximation, the electric field amplitude $\vec{F}_s(z)$ of the probe beam with wave vector $k_s$ behind the interaction zone of length $l$ is given by

$$\vec{F}_s(l) = F_s(0) \frac{1}{\sqrt{2}} \left[ \vec{e}_+ + \vec{e}_- \left( 1 + i\Delta\eta_s k_s l \right) \right]. \qquad \text{(A5)}$$

This results in a phase shift of the $\vec{e}_-$ component, which causes a rotation of the polarization direction of the probe beam by a small angle $\theta_s = \Delta n_s k_s l/2$, together with absorption, which yields slightly elliptic polarization, the ratio of minor to major axis of the ellipse being $r_s = \Delta\kappa_s k_s l/2$. The projections of $\vec{F}_s(l)$ on the $y$ and the $x$ axis determine the ratio of the corresponding irradiances $E \propto |\vec{F}|^2$, where $E_y$ is the irradiance passing an analyzing polarizer and $E_x$ is reflected. In the weak absorption regime, $E_x$ can be taken to be equal to the unperturbed irradiance $E_s$ before the interaction and $E_y$ is $(\theta_s^2 + r_s^2) E_s$. Denoting $E_y$ by $\delta E_s$, we find

$$\frac{\delta E_s}{E_s} = \frac{1}{16} \left( \sigma_{S \rightarrow S}^{(2)} g^{(2)} N_i \frac{E_p l}{\hbar \omega_p} \right)^2 P(\Delta\omega) + R. \qquad \text{(A6)}$$

Here, $R$ represents the residual transmission of the crossed polarizers, i.e., $\delta E_s/E_s$ as measured without pump beam, and $P(\Delta\omega)$ is the line shape function as

given in Eq. (A8). In the experiment, the detectors integrate over the whole spatial and temporal profile of the probe beam, and corresponding mean values have to be used in Eq. (A6), i.e., the product of $E_p$ and $l$ has to be replaced by a suitably defined mean value $\langle E_p l \rangle$. This leads to Eq. (1) in Sec. II. For the case of an $S \rightarrow D$ transition, the different polarization dependence, Eq. (A3), leads to an additional factor of 5/4 inside the large bracket.

The windows that close the plasma chamber also show a minor anisotropy and cause an extra phase shift and absorption of one of the polarization components. The corresponding changes of the probe beam polarization may be described by $\theta_w$ and $r_w$. Since the window anisotropies always act on the same polarization component of the probe beam, their effect can largely be reduced by combining measurements with left and right circularly polarized pump beam, which lead to total turning angles of $\theta_w \pm \theta_s$ (and vice versa for $r$). Therefore, every signal was measured twice, with $\vec{e}_p = \vec{e}_+$ as well as with $\vec{e}_p = \vec{e}_-$. The mean value of the two signals is

$$\frac{1}{2} \left[ \left( \frac{\delta E_s}{E_s} \right)_+ + \left( \frac{\delta E_s}{E_s} \right)_- \right] = \theta_s^2 + r_s^2 + (\theta_w^2 + r_w^2 + R).$$

$$\text{(A7)}$$

By this method, the window anisotropy merely results in an effective increase of the residual transmission but does not influence the signal itself. The accuracy requirements for the circular polarization of the pump beam are not very high. A small additional component $\epsilon$ of the wrong circular polarization, i.e., $\vec{e}_p = \vec{e}_+ + \epsilon\vec{e}_-$, reduces the signal only by a factor $(1 - \epsilon^2)^2$, which leads to an overestimation of $N_i$ by a factor of $1/(1 - \epsilon^2)$.

The line shape function $P(\Delta\omega)$ (with SI unit $s^2$) is the sum of the squares of the absorption and dispersion line shapes, which are connected by a Kramers-Kronig relation. The explicit expression for $P$ in Eq. (A6) in terms of the two-photon absorption line shape $L$ from Eq. (A1) is

$$P(\Delta\omega) = L(\Delta\omega)^2 + \left[ \frac{1}{\pi} \, \text{P} \int_{-\infty}^{\infty} \frac{L(\omega + \omega_p - \omega_0)}{\omega - \omega_s} d\omega \right]^2.$$

$$\text{(A8)}$$

In the cases of a Lorentz, a Gauss and a Voigt profile $L$, the relation between $L$ and $P$ is as follows:

$$L(\Delta\omega) = \frac{1}{\pi}\frac{\Gamma}{\Delta\omega^2 + \Gamma^2}$$

$$\to P(\Delta\omega) = \frac{1}{\pi^2}\frac{1}{\Delta\omega^2 + \Gamma^2},$$

$$L(\Delta\omega) = \frac{1}{\sqrt{\pi}\gamma}\exp\left(-\frac{\Delta\omega^2}{\gamma^2}\right)$$

$$\to P(\Delta\omega) = \frac{1}{\pi\gamma^2}\left|\exp\left(-\frac{\Delta\omega^2}{\gamma^2}\right) + i\frac{2}{\sqrt{\pi}}\mathcal{F}\left(\frac{\Delta\omega}{\gamma}\right)\right|^2,$$

$$L(\Delta\omega) = \frac{1}{\sqrt{\pi}\gamma}\text{Re}\left[w\left(\frac{\Delta\omega + i\Gamma}{\gamma}\right)\right]$$

$$\to P(\Delta\omega) = \frac{1}{\pi\gamma^2}\left|w\left(\frac{\Delta\omega + i\Gamma}{\gamma}\right)\right|^2. \tag{A9}$$

In these equations, $\mathcal{F}$ is the Dawson integral and $w(z) = \exp(-z^2)\text{erfc}(-iz)$ is related to the complex error function [37]. For all three profiles, the original normalization to unit area is lost after the transformation. In the far wing, the dispersion part of $P$ dominates and all three profiles decrease as $1/(\pi\Delta\omega)^2$. For data evaluation the spectra were fitted with the function $A^2 P(\Delta\omega) + R$ with the fixed measured value $R$ of the residual transmission (including window effects). The resulting value of $A^2$ is just the prefactor of $P$ in Eq. (A6). The quantity $2A$ is the probe beam absorption [see Eq. (A4)], integrated over the whole line, and thus provides a measure of the number density of the absorbing particles independent of the line shape.

The full width at half maximum (FWHM) for a Voigt profile is in good approximation given by

$$\text{FWHM} = \Gamma + \sqrt{\Gamma^2 + (2.0125\gamma)^2}, \tag{A10}$$

which includes the special cases of the Lorentz and Gauss profile. If the approximation of monochromatic laser beams is not satisfied, the absorption and dispersion pro-files have to be convolved with the spectral profile of the pump laser. The resulting profile is then to be convolved with the spectral profile of the signal laser. Since the width of our signal laser is a factor of five smaller than the width of our pump laser, we could always treat the signal laser as a monochromatic light source.

Asymmetric Lorentz profiles, as they are observed for pressure broadened spectral lines, lose the asymmetry by the transformation from $L$ to $P$.

$$L(\Delta\omega) = \frac{1}{\pi}\frac{\Gamma + \kappa\Delta\omega}{\Delta\omega^2 + \Gamma^2} \to P(\Delta\omega) = \frac{1}{\pi^2}\frac{1 + \kappa^2}{\Delta\omega^2 + \Gamma^2}. \tag{A11}$$

Thus, the asymmetry factor $\kappa$ cannot be detected by polarization spectroscopy and has to be measured differently if it is required for evaluation of the number density. This is not a serious complication, however, because $\kappa$ is usually small and can be neglected if it is less then about 10% (see Sec. IV). Convolution of the asymmetric Lorentz profile with a Gauss profile leads to the Voigt result [third line in Eq. (A9)] with an extra factor of $1 + \kappa^2$.

[1] C. J. Dash and J. H. Bechtel, Opt. Lett. 6, 36 (1981).
[2] R. E. Teets and J. H. Bechtel, Opt. Lett. 6, 458 (1981).
[3] C. P. Auschnitt, G. C. Björklund, and R. R. Freeman, Appl. Phys. Lett. 33, 851 (1978).
[4] J. E. M. Goldsmith, Opt. Lett. 7, 437 (1982).
[5] K. C. Smyth and P. J. H. Tjossem, Appl. Phys. B 50, 499 (1990).
[6] J. Bokor, R. R. Freeman, J. C. White, and R. H. Storz, Phys. Rev. A 24, 612 (1981).
[7] U. Meier, K. Kohse-Hoinghaus, and T. Just, Chem. Phys. Lett. 126, 567 (1986).
[8] J. T. Salmon and N. M. Laurendeau, Opt. Lett. 11, 419 (1986).
[9] J. E. M. Goldsmith, Appl. Opt. 28, 1206 (1989).
[10] J. Bittner, K. Kohse-Hoinghaus, U. Meier, and T. Just, Combust. Flame 71, 41 (1988).
[11] U. Meier, K. Kohse-Hoinghaus, L. Schafer, and C. P. Klages, Appl. Opt. 29, 4993 (1990).
[12] Ph. Mertens and P. Bogen, Appl. Phys. A 43, 197 (1987).
[13] M. Aldén, H. Edner, P. Grafström, and S. Svanberg, Opt. Commun. 42, 244 (1982).
[14] W. K. Bischel, B. E. Perry, and D. R. Crosley, Appl. Opt. 21, 1419 (1982).
[15] D. J. Bamford, L. E. Jusinski, and W. K. Bischel, Phys. Rev. A 34, 185 (1986).
[16] S. Agrup, U. Westblom, and M. Aldén, Chem. Phys. Lett. 170, 406 (1990).
[17] K. Danzmann, K. Grützmacher, and B. Wende, Phys. Rev. Lett. 57, 2151 (1986).
[18] J. Seidel, Phys. Rev. Lett. 57, 2154 (1986).
[19] D. Heiman, R. W. Hellwarth, M. D. Levenson, and G. Martin, Phys. Rev. Lett. 36, 189 (1976).
[20] R. Loudon, The Quantum Theory of Light, 2nd ed. (Clarendon Press, Oxford, 1983).

[21] H. D. Simaan and R. Loudon, J. Phys. A **8**, 1140 (1975).

[22] T. D. Raymond, N. Böwering, Chien-Yu Kuo, and J. W. Keto, Phys. Rev. A **29**, 721 (1984).

[23] S. Kröll and W. K. Bischel, Phys. Rev. A **41**, 1340 (1990).

[24] M. D. Plimmer and P. E. G. Baird *et al.*, J. Phys. B **22**, L241 (1989).

[25] J. Szudy and W. E. Baylis, J. Quant. Spectros. Radiat. Transfer **15**, 641 (1975).

[26] J. Szudy and W. E. Baylis, J. Quant. Spectros. Radiat. Transfer **17**, 681 (1977).

[27] K. Grützmacher and B. Wende, Phys. Rev. **A 16**, 2140 (1978).

[28] K. Grützmacher and A. Steiger, in *Spectral Line Shapes*, edited by J. Szudy (Ossolineum, Wrocław, 1988), Vol. 5, pp. 35–48.

[29] C. R. Vidal, J. Cooper, and E. W. Smith, Astrophys. J. Suppl. (No. 214) **25**, 37 (1973).

[30] K. Behringer, Appl. Phys. **20**, 19 (1979).

[31] K. Behringer and N. van Cung, Appl. Phys. **22**, 373 (1980).

[32] F. Bassani, J. I. Forney, and A. Quattropani, Phys. Rev. Lett. **39**, 1070 (1977).

[33] R. W. Ditchburn and U. Öpik, in *Atomic and Molecular Processes*, edited by D. R. Bates (Academic Press, New York, 1962), pp. 79–96.

[34] M. A. Clyne and W. S. Nip, in *Reactive Intermediates in the Gas Phase*, edited by D. W. Setser (Academic Press, New York, 1979), pp. 1–57.

[35] D. C. Hanna, M. A. Yuratich, and D. Cotter, *Nonlinear Optics of Free Atoms and Molecules* (Springer-Verlag, Berlin, 1979).

[36] W. Demtröder, *Laserspektroskopie*, 2nd ed. (Springer-Verlag, Berlin, 1991).

[37] W. Gautschi, in *Handbook of Mathematical Functions*, edited by M. Abramowitz and I. A. Stegun, 9th print. (Dover Publications, New York, 1964), pp. 297–329.